Journal Pre-proofs

Kinetics of hydrothermal reactions of n-butanol over Pt/Al_2O_3 catalyst for bio-propane fuel gas production

Seyed Emad Hashemnezhad, Jude A. Onwudili, Patricia Thornley, Keith E. Simons

PII: S1385-8947(24)08816-8
DOI: https://doi.org/10.1016/j.cej.2024.157325
Reference: CEJ 157325

To appear in: *Chemical Engineering Journal*

Received Date: 25 July 2024
Revised Date: 3 October 2024
Accepted Date: 31 October 2024

Please cite this article as: S.E. Hashemnezhad, J.A. Onwudili, P. Thornley, K.E. Simons, Kinetics of hydrothermal reactions of n-butanol over Pt/Al_2O_3 catalyst for biopropane fuel gas production, *Chemical Engineering Journal* (2024), doi: https://doi.org/10.1016/j.cej.2024.157325

Kinetics of hydrothermal reactions of n-butanol over Pt/Al_2O_3 catalyst for biopropane fuel gas production

Seyed Emad Hashemnezhad [1], Jude A. Onwudili [1,2,*], Patricia Thornley [1], Keith E. Simons [3]

[1] Energy and Bioproducts Research Institute, College of Engineering and Physical Sciences, Aston University, Birmingham B4 7ET, UK

[2] Department of Chemical Engineering and Applied Chemistry, College of Engineering and Physical Sciences, Aston University, Birmingham B4 7ET, UK

[3] Futuria Fuels, SHV Energy, 2132 JL Hoofddorp, the Netherlands

Abstract

Energy defossilisation using drop-in biofuels is an important step towards Net Zero. Producing low-carbon clean-burning propane fuel from biomass provides such additional sustainability benefits. In this work, kinetics of hydrothermal reactions of n-butanol, a biomass-derived feedstock, to produce propane over 5wt% Pt/Al_2O_3 catalyst have been studied from 523- 573 K. Experimental data revealed negligible internal and external mass transfer effects and, when fitted to an integral power-rate law equation, gave activation energy of 70 kJ mol^{-1} (n-butanol reaction order =1). Furthermore, an appropriate Langmuir-Hinshelwood model was developed, which predicted similar activation energy 62 kJ mol^{-1}. Low adsorption enthalpies for n-butanol (-33.51 kJ mol^{-1}) and water (-18.16 kJ mol^{-1}) indicated weak interactions on the catalyst surface. These agreed with the fast reaction rate of ≈1.0 x 10^{-5} mol g_{cat}^{-1} s^{-1} obtained at ≥ 548 K. As a new research area, generation of such accurate kinetics data will contribute to process development for large-scale biopropane production.

Keywords: Biomass, Biobutanol, Biopropane, Reaction kinetics, Catalytic hydrothermal reaction, Defossilisation

* Corresponding author at: Energy and Bioproducts Research Institute, College of Engineering and Physical Sciences, Aston University, Birmingham B4 7ET, UK.

E-mail addresses: 220258773@aston.ac.uk (Seyed Emad Hashemnezhad), j.onwudili@aston.ac.uk (J.A. Onwudili), Patricia Thornley (p.thornley@aston.ac.uk), keith.simons@futuriafuels.com (K.E. Simons),

1. Introduction

In 2023 international scientific experts reported that the 1.5 °C warming limit set out in the Paris Agreement will be reached by the early 2030s in line with the current warming rate [1]. This will make this current decade crucial for reducing emissions of carbon dioxide and other greenhouse gases (GHG). Among the commercial fossil fuels, liquefied petroleum gases (LPG), consisting mainly of propane and butane, are known for their cleaner combustion and significantly lower emissions. LPG emits 33% less carbon compared to coal [2], 74% less nitrogen oxides (NO_X) and 81% less particulate matter (PM) compared to diesel [3], and 100% less sulphur oxides (SO_X) compared to heating oil [4]. At present, the global demand for LPG stands at over 300 million tonnes each year [5]. Despite their lower carbon intensity compared to other fossil fuels used in transportation and heating, combustion of fossil-derived LPG still contributes significantly to overall global CO_2 emissions.

Biomass-derived fuels can play a crucial role in reducing carbon emissions and promoting sustainability by offering a renewable alternative to fossil fuels in the energy sector. Biomass-derived LPG (Bio-LPG) is an attractive biofuel that combines the beneficial features of LPG, such as low emissions, cleaner burning, versatility, and portability, with the added advantage of being a low-carbon fuel. In comparison to fossil-derived LPG whose large-scale deployment can effectively contribute to short-term emission targets [6], switching to Bio-LPG can further reduce the GHG emissions by up to 78% while producing the same low NO_X, SO_X, and PM as fossil-derived LPG [7]. Thus, producing LPG component gases from biomass presents an opportunity for enhanced sustainability gains. Currently, Bio-LPG has been specially recognized both by Liquid Gas UK (LGUK) and the World Liquid Gas Association (WLGA) as a potential solution to reducing carbon emissions for the difficult-to-decarbonise sectors including off-grid locations [8, 9]. However, this product is currently available only in limited commercial quantities compared to global fossil market. It is derived as a by-product, yielding 5–8 % biopropane, from renewable diesel and Sustainable Aviation Fuel (SAF) production, via hydrotreating of vegetable oils and fats (HVO) [10].

Significant research activities are currently taking place to develop on-purpose production routes for Bio-LPG using biomass derived feedstocks. Typical feedstocks include C_4-C_5 carboxylic acids such as butyric acid [11], levulinic acid [12] and alcohols such as glycerol [13, 14], ethanol [15] and n-butanol [16]. N-butanol can be obtained commercially from biomass via the acetone-butanol-ethanol (ABE) fermentation [17] and novel non-fermentative routes [18]. Recently, Diejomaoh et al. [16] investigated the hydrothermal reactions of n-butanol over 5wt% Pt/Al_2O_3 over a temperature range of 473 K to 623 K and reported the optimal conditions to be 573 K and 1 hour reaction time. The authors used the experimental data to explain that decarbonylation and/or deformylation were the main reaction mechanisms that led to high yields of propane, along with CO_2 and hydrogen gas [16]. The specific activity of the Pt/Al_2O_3 catalyst has been previously demonstrated by Lercher and coworkers [19, 20], who showed that this catalyst could selectively convert n-propanol to mainly ethane by preventing excessive C–C bond cleavage. Reportedly Pt was able to facilitate key reactions such as (de)hydrogenation and decarbonylation, resulting in the formation of alkanes with one fewer carbon atom from aliphatic alcohols [19, 20]. Furthermore, the use of metal oxide supports such as alumina can enhance synergistic catalysis during hydrothermal processing [16, 21, 22]. In addition, such supports offer the possibility of catalyst regeneration via combustion [16], which is often difficult with other supports commonly used in hydrothermal media such as activated carbon [11].

With the promising results of the thermodynamic study of butanol conversion to propane [16, 22], it is equally important to understand the reaction kinetics to enhance the potential of this process for further optimisation and development. While multiple studies have examined the reaction kinetics of n-butanol reforming over various transition metal catalysts [23-25], the specific kinetics of n-butanol hydrothermal reaction for on-purpose production of propane is notably absent in the literature. To bridge this knowledge gap, this present study has systematically examined this reaction under various reaction temperatures (523 K - 573 K) and reaction times (0 - 45 minutes) over 5wt% Pt/Al_2O_3 using a batch reactor to produce crucial kinetic data. The internal and external mass transfer were adequately assessed to ensure that data was collected within the kinetically controlled regime. The kinetic data was subsequently used to evaluate the applicability of the power rate law in describing the reaction rate and to determine the apparent activation energy of the reaction. In addition, a kinetic model based on the Langmuir-Hinshelwood mechanism was developed, and its fit to the experimental data was established. Establishing these kinetic data would be essential for predicting reaction behaviour under various conditions, enabling better control of the process for optimal yield and selectivity, and providing crucial data for efficiently and safely scaling up the process.

2. Materials and Methods

2.1. **Materials**

N-butanol (99% extra pure) was obtained from Acros Organics. Ethyl acetate (≥99%, laboratory reagent grade), was obtained from Fisher Chemical. 5 wt% Pt/$\mathbf{Al_2O_3}$ was purchased from Catal International Limited, Sheffield, UK. The catalyst characteristics previously reported in a prior publication include a bulk density of 720 kg $\mathbf{m^{-3}}$, actual Pt metal content of 5.07 wt%, average particle size of 30 µm, BET surface area of 182 m^2 g^{-1}, pore volume of 0.7 $\mathbf{cm^3\ g^{-1}}$ and pore diameter of 9.00 nm [26]. Deionized water was produced in-house using a Milli-Q Advantage A10 Water Purification System. All the materials were used as received.

2.2. Methodology

2.2.1. Batch reactor procedure

The schematic of the experimental procedure for the catalytic hydrothermal reaction of n-butanol is presented in Fig. 1.

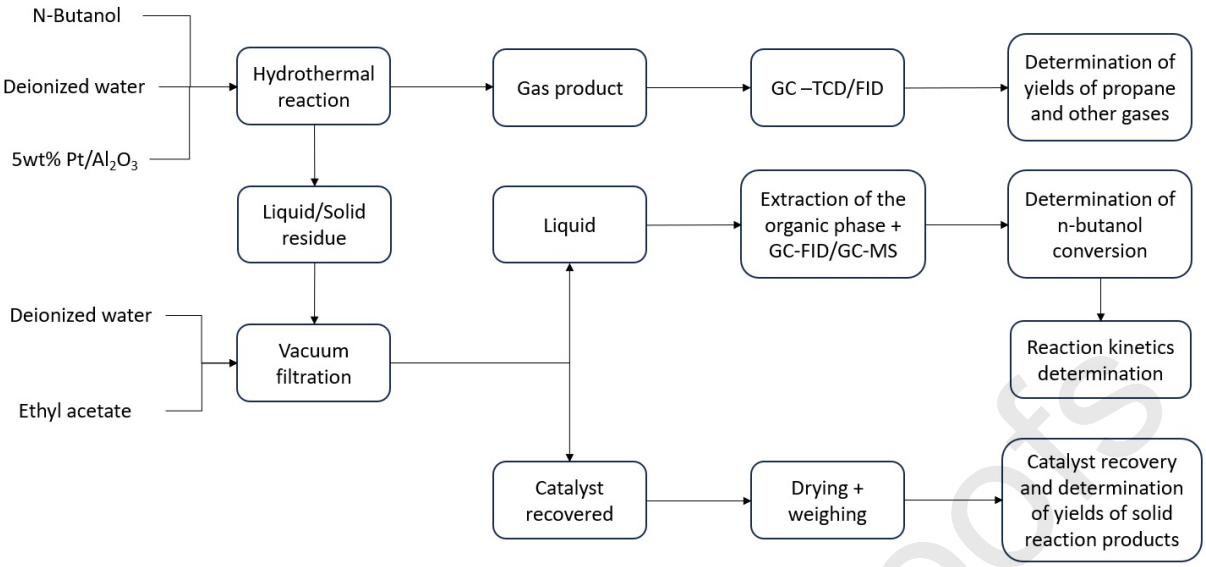

Fig. 1. The schematic of the experimental procedure for the catalytic hydrothermal reaction of n-butanol.

The basis of experimental procedure has been reported previously [16]. In summary, the catalytic hydrothermal reaction of n- butanol was carried out in a 100 mL capacity batch reactor obtained from Parr Instruments Co. Inc. Moline, Illinois, USA. The reactor can operate at a maximum temperature of 873 K and a pressure of 345 bar. Additionally, some experiments were performed using a stirred 100 mL batch reactor, also from Parr Instruments, which can operate at a maximum temperature of 773 K and the pressure of 345 bar. For each experiment, 18 g of deionised water and 2 g of butanol (to give 10 wt% n-butanol aqueous solution) was weighed out in a beaker and loaded into the reactor, followed by the addition of the various amount of catalyst (0.1 g to 1 g). After loading, the reactor was sealed and gently purged three times with nitrogen followed by pressurization to 5 bar using the same nitrogen. The nitrogen served to provide inert reaction environment, maintain accurate pressure measurements during experiments and standardize gas analysis. Subsequently, the reactor was inserted into an electric heating jacket equipped with a temperature controller and gradually heated to desired temperature at a rate of about 10 K per minute. At the conclusion of each run, the reactor was removed from the heating jacket and rapidly cooled to ambient temperature within 5 minutes using a cold-water bath.

Once cooled, the pressure and temperature of the reactor were recorded, followed by the collection of the gas product using 1 L Tedlar bag for immediate analysis via GC-FID/TCD. The reactor was then opened, and the slurry consisting of both liquid and solid components (mainly the catalyst), was poured directly into a filtration assembly equipped with Whatman Grade 4 qualitative filter paper. The reactor then was rinsed with 20 ml of deionized water followed by 20 ml of ethyl acetate to ensure complete slurry collection. The recovered catalyst was dried on a hotplate at 378 K overnight and then weighed for mass balance calculations. The liquid sample consisting of unreacted n-butanol was analysed by GC-FID to enable the calculation of n-butanol conversion. Repeated experiments showed a standard deviation of less than $\pm$ 5% for the conversion of n-butanol and the gas product yield, indicating good reproducibility of the experimental measurements.

2.2.2. Analysis of gas phase products

The gas analysis procedure used in this study was previously validated and published in earlier studies [11, 16, 27]. Briefly, a Shimadzu GC-2014 gas chromatograph equipped with two injection ports, two columns and two detectors were used to analyse the gas samples. The injectors were maintained at a temperature of 333 K, while the detectors, comprising a flame ionization detector (FID) and a thermal conductivity detector (TCD), were set at 493 K. The procedure involved injection of 0.6 mL of the gas sample using a gas-tight syringe. The column oven program initiated at 353 K and followed a gradual increase to 453 K at a rate of 10 K per minute, after which it was held at 453 K for 3 minutes. This protocol resulted in a total analysis duration of 13 minutes. For the separation of hydrocarbons, a Hayesep column with a mesh size of 80–100, measuring 2 mm in diameter and 2 m in length, was used. Quantification was performed using the FID for hydrocarbons. Separation of Permanent gases (H_2, N_2, CO and CO_2) was done using a molecular sieve column with 60–80 mesh range, with a diameter of 2 mm and a length of 2 m. Quantification of these gases were done using the TCD.

The percentage volume of each gas obtained from their peak area was used to calculate the mole of each gas component by employing the Ideal Gas Law using Equation (1):

$$\text{Mole of each gas component, } n_i = \left(\frac{P_i \times V}{RT}\right) \quad (1)$$

where n_i is the mole of each gas component (mol), P_i is the partial pressure of each gas component (volume fraction of each gas component × reactor pressure after cooling (Pa)), V is the volume of the reactor headspace (m^3), R is the general gas constant (8.314 J mol^{-1} K^{-1}), and T is the reactor ambient temperature after cooling (K).

The individual molar gas yield (%) then is calculated using Equation (2):

$$\text{Individual gas component molar yield (\%)} = \left(\frac{n_i}{n_{butanol}}\right) \times 100 \quad (2)$$

where $n_{butanol}$ represents the number of moles of butanol in the feed.

Turnover frequency (TOF) with respect to propane production was calculated based on Equation (3).

$$\text{Propane TOF } (min^{-1}) = \frac{\text{Moles of propane produced per minute}}{\text{Moles of surface metal present in the reactor}} \quad (3)$$

Considering the gas products were held under pressure (~5-6 bar N_2), the moles of dissolved CO_2 were calculated using Henry's law [27].

2.2.3. Analysis of liquid phase products

Analysis of the liquid residuals followed the procedure previously described by Diejomaoh et al., [16]. The organic phase was extracted with 1 x 20 ml and 2 x 5 ml aliquots of ethyl acetate and analysed using a Shimadzu GC-2010 with a ZB-50 capillary column (0.32 mm inner diameter, 30 m length) and a flame ionization detector (FID). Helium was used as the carrier gas at a flow rate of 2.12 mL min^{-1}. A 1 μL sample was injected at 553 K with a 20:1 split ratio. The column oven was initially at 323 K for 5 minutes, then ramped at 10 K min^{-1} to 553 K, held for 2 minutes. The total analysis time was 30 minutes. Additionally, a Shimadzu GC-2010 Plus combined with a Shimadzu Single Quadrupole Mass Spectrometer (QP2010 SE) was utilized to analyse a few samples to identify possible byproducts. The DB-5 ms capillary column used had a 0.25 mm inner diameter and 30 m length, with a helium flow rate of 1.5 mL min^{-1}, the same sample volume and injection port temperature as the GC-FID, and a 50:1 split ratio. The column oven program was identical to the GC-FID. Compounds were detected using a mass selective (MS) detector at 523 K, with a transfer line at 548 K. Mass spectra were generated with 70 eV ionization energy, covering m/z = 35–300, with a scan time of 0.35 s. The National Institute of Standards and Technology (NIST, 2020 Version) library installed on the MS was used to identify the peaks. Quantitative analysis of n-butanol was carried out using an external standard method. Briefly, four samples, each containing a known amount of n-butanol and ethyl acetate, were prepared and used to plot a 4-point calibration curve of the mass fraction of n-butanol against the GC-FID peak area. The extracted organic phase, containing mainly unreacted n-butanol, was then quantified using the prepared calibration data. The conversion of n-butanol was calculated using Equation (4):

$$\text{Conversion}(\%) = \frac{\text{mole of butanol feed} - \text{mole of unreacted butanol}}{\text{mole of butanol feed}} \times 100 \quad (4)$$

With water as an excess component in the feed, the concentration of n-butanol in the recovered liquid sample was calculated using the Equation (5):

$$\text{Concentration}\ (\text{mol L}^{-1}) = \frac{\text{mole of unreacted butanol}}{\text{Volume of the solution}} \quad (5)$$

3. Results and discussion

3.1. Mass Transfer

The catalytic hydrothermal reaction of liquid n-butanol to produce gases in the presence of solid 5wt% Pt/Al_2O_3 catalyst is a heterogeneous reaction. Such processes involve the transfer of reactants from the gas-liquid phase to the catalyst surface, diffusion through the catalyst pores, and reaction at the active sites, followed by the diffusion of the products. The reaction rate in this gas-liquid-solid three-phase system can be affected by both internal and external mass transfer limitations. Therefore, prior to evaluation of the experimental data used for the reaction kinetic study, it was essential to address the absence of internal and external mass transfer limitations, which will be discussed in this section.

197

198 **3.1.1. Assessment of internal mass transfer limitation**

199 To validate the absence of internal mass transfer limitation, the Weisz-Prater criterion was used
200 [28]. In a kinetically controlled regime free of pore diffusion limitation, as per this method, the
201 value of the Weisz-Prater modulus (Φ) (6) should be below 6 for zero-order reaction, below
202 unity for first-order reaction, and below 0.3 for second-order reaction.

$$\Phi = \frac{r_{obs} R^2}{c D_{eff}} \quad (6)$$

203 In Equation (6) r_{obs} is the maximal initial reaction rate (mol $L^{-1}s^{-1}$), R is the mean radius of
204 the catalyst particle (m), c is the substrate concentration (mol L^{-1}) and D_{eff} is the effective
205 diffusion coefficient of the substrate ($m^2\ s^{-1}$).

206 The effective diffusion coefficient (D_{eff}) can be defined as follows: $D_{eff} = D\ (\xi/\chi)$, where D
207 represents the substrate (n-butanol) diffusion coefficient in the liquid phase (water), ξ denotes
208 catalyst porosity, and χ indicates catalyst tortuosity. The diffusion coefficient (D) can be
209 obtained from the Wilke−Chang equation (7) [29]:

$$D^{o}_{AB} = \frac{7.4 \times 10^{-8} (\phi M_B)^{\frac{1}{2}} T}{\eta_B V^{0.6}_{b(A)}} \left[\frac{cm^2}{s}\right] \quad (7)$$

210 Where ϕ is the dimensionless association factor (for water, ϕ = 2.6), M_B is the molecular
211 weight of the solvent (water = 18 g mol^{-1} η_B is the solvent dynamic viscosity at reaction
212 temperature T (K) (water = 0.0912 cP at T = 573 K) and $V_{b(A)}$ is the liquid molar volume at the
213 solute's normal boiling point. $V_{b(A)}$ can also be written as $0.285 \times V_{c(A)}^{1.048}$, where $V_{c(A)}^{1.048}$ is the
214 solute critical volume (n-butanol = 275 $cm^3\ mol^{-1}$). When inputting the values for the
215 diffusion of n-butanol in water at T = 573 K and P = 90 bar, the resulting diffusion coefficient
216 (D^{o}_{AB}) was calculated to be $1.632 \times 10^{-8} m^2\ s^{-1}$.

217 From dividing the pore volume by the total volume, the catalyst porosity (ξ) was calculated to
218 be 0.504. The typical values for the catalyst tortuosity (χ) can vary from 2 to 5. By assuming
219 the $\xi/\chi = 0.1$ which has been reported for 5 wt% Pt/Al_2O_3 catalyst in the literature [30], the
220 effective diffusion coefficient (D_{eff}) of n-butanol at T = 573 K and P = 90 bar was calculated
221 to be $1.632 \times 10^{-9}\ m^2\ s^{-1}$. The upper limit of tortuosity of 5 was used in this case, which
222 resulted in the smallest possible D_{eff} and the largest possible but satisfactory value of the Weisz-
223 Prater criterion (Φ). Therefore, if the upper limit of the tortuosity satisfied Φ, then lower values
224 would also meet the condition.

225

226 The maximum initial reaction rate (r_{obs}) for the hydrothermal reaction of n-butanol was $4.83 \times$
227 10^{-4} mol L^{-1} s^{-1} at T = 573 K and concentration (c) of 0.69 mol L^{-1} of n-butanol. The mean
228 radius of the catalyst particle reported in prior publication was 1.5×10^{-5}m [26]. Inputting

these values into equation (6) gave the value of 9.64×10^{-5} for the Weisz-Prater modulus (Φ). The obtained value confirmed the absence of the internal mass transfer and pore diffusion for the condition used in this study.

The obtained Weisz-Prater modulus (Φ) and the confirmation of the absence of internal mass transfer are consistent with results reported in the literature from closely related studies. For example, Yadav et al. [23] evaluated the internal mass transfer limitation of steam reforming of n-butanol using a fixed bed reactor over 0.5 wt% Pt/Al_2O_3. They reported the value of $\Phi = 2.81 \times 10^{-4}$ at T = 773 K and $W/F_{A0} = 33.4$ g h mol^{-1}, hence concluded that the pore diffusion did not affect the reaction rate. In the case of higher Pt loading used in this present study, Wärnå et al. [30] showed that no transport limitation occurred in reforming of sorbitol over 5 wt% Pt/Al_2O_3. They obtained a value of $\Phi = 0.005$ at 498 K and 30 bar using a fixed-bed reactor setup for 0.515 mol L^{-1}concentration of feed [30].

3.1.2. Assessment of the external mass transfer limitation

To evaluate the effect of external mass transfer limitation, separate reactions with varying catalyst masses ranging from 0.1 to 1 g were conducted at 573 K for 15 minutes of reaction time. As depicted in Fig. 2, the turnover frequency (TOF) of propane slightly increased from 0.3 to 0.34 min^{-1} when the catalyst mass was increased from 0.1 to 0.5 g. This slight increase possibly indicated an enhancement in external mass transfer due to better availability of catalyst active sites for the reaction. However, a further increase in catalyst mass to 0.75 and 1 g resulted in a decrease in propane TOF to 0.22 and 0.19 min^{-1}, respectively, suggesting the presence of external mass transfer limitations. This decrease could be due to overcrowding of catalyst particles, leading to restricted access of reactants to the active sites, or an increase in the thickness of the catalyst bed, which hindered effective reactant diffusion. Given that the change in propane TOF was minimal between 0.1 and 0.5 g catalyst loading, it could be concluded that external mass transfer limitations did not significantly affect the reaction rates for the amount of catalyst used in this study (0.5 g). In a similar approach, Yadav et al. [23] demonstrated that the turnover frequencies of H_2 were independent of the catalyst mass, which ranged from 0.5 to 1.5 g. This was observed for a fixed feed flow rate of 1 cm^3/min at a temperature of 773 K during the steam reforming of n-butanol. Consequently, they concluded that external mass transfer limitation was absent in their system.

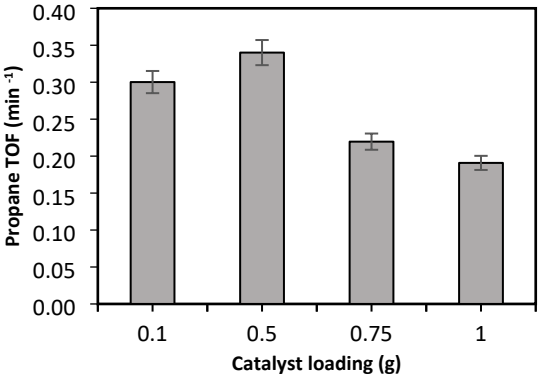

Fig. 2. Variation of the propane TOF with varying catalyst mass (Reaction conditions: t = 15 min, T = 573 K, initial N_2 pressure = 5 bar).

In addition to catalyst loading, the effect of agitation speed on external mass transfer was evaluated using a stirred reactor with 0.5 g of catalyst at 573 K for a reaction time of 15 minutes. As shown in Fig. 3, stirring caused a significant decrease in propane TOF, dropping from 0.34 min^{-1} (non-stirred reactor) to 0.06 min^{-1} at 350 rpm. Although the TOF improved as the agitation speed increased to 1100 rpm, reaching 0.16 min^{-1}, it remained significantly lower than the non-stirred system. Even at 1850 rpm, where the TOF stabilized at 0.18 min^{-1}, it was still below that of the non-stirred reactor. One possible explanation for the decrease in TOF upon stirring is that mechanical agitation caused catalyst particles to stick together around the more stable centre of the vessel, which experiences lower pressure due to a combination of centrifugal forces, vortex formation and fluid dynamics. These phenomena would cause poor catalyst particle distribution in the aqueous medium, resulting in less contact between catalyst surface and the reactant molecules that are more dispersed in the agitated fluid. Indeed, higher stirring rate helped more catalyst dispersion but to a lesser extent compared to the natural convection patterns formed in the hydrothermal environment. Therefore, due to the persistently lower TOF observed in the stirred reactor, subsequent experiments were conducted using the non-stirred reactor.

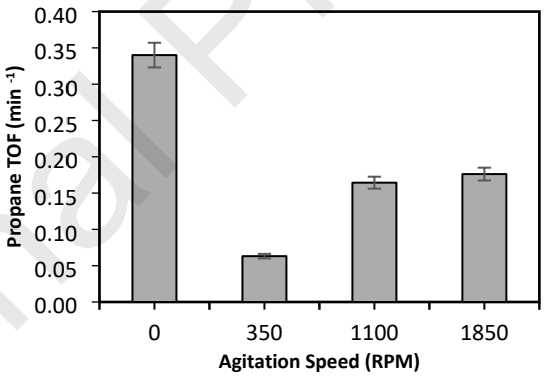

Fig. 3. Variation of the propane TOF with varying agitation speed (Reaction conditions: t = 15 min, T = 573 K, initial N_2 pressure = 5 bar).

3.2. Formation of the products during hydrothermal reaction of n-butanol

Fig. 4 depicts the changes in the feed concentrations and products molar yield during the catalytic hydrothermal reaction of n-butanol. In this case, the amount of 5 wt% Pt/Al_2O_3 used was 0.5 g and the set temperature was 573 K in all experiments. The reaction times were varied from 0 min to 45 min with "0 min" referring to the experiments that were quickly quenched once the set temperature was reached. As shown in Fig. 4a, the decrease in n-butanol concentration was rapid with the reaction rate being diminished close to 45 min of reaction time. The main products formed as depicted from gases molar yield (Fig. 4a) were hydrogen, carbon dioxide and propane. The average molar yield ratios of the main products within the reaction time investigated were as follows: $CO_2 : C_3H_8$ = 1.07, $H_2 : C_3H_8$ = 2.03, $H_2 : CO_2$ =

1.89. The ratios indicate that the reaction pathway presented in Equation (8) can reliably describe the formation of the main products under the reaction condition investigated in this work.

$$C_4H_9OH + H_2O \rightarrow C_3H_8 + CO_2 + 2H_2 \qquad (8)$$

Multiple possible reaction mechanisms could lead to the formation of the main products according to Equation (8). These pathways are depicted in Table 1. The first possible pathway involves the initial dehydrogenation of n-butanol to butanal, followed by the decarbonylation of butanal to propane and carbon monoxide. Carbon monoxide then undergoes the water-gas shift reaction to produce carbon dioxide and an additional mole of hydrogen. This mechanism has been proposed in various studies [16, 19, 20, 31, 32]. A recent study by Diejomaoh et al. [16], suggested this mechanism as one of the dominant pathways for the formation of propane, hydrogen, and carbon dioxide in the hydrothermal reaction of n-butanol over a Pt/Al_2O_3 catalyst. Additionally, in a study on the aqueous-phase reforming of n-butanol over Ni/Al_2O_3 and Ni/CeO_2, Roy et al. [32] indicated the possible formation of propane through this mechanism, as evidenced by the presence of butanal in their liquid analysis. Peng et al. [20] proposed the dehydrogenation/decarbonylation pathway as a potential mechanism due to the observation of trace amounts of propanal during the hydrodeoxygenation of n-propanol over a Pt/Al_2O_3 catalyst. Analysis of the liquid product from this present study (see *Supplementary Information Figure S1*) also showed minor formation of butanal, further confirming the possible occurrence of this reaction pathway.

Another mechanism, previously described by Diejomaoh et al. involves the possible direct deformylation of n-butanol to propane and formaldehyde, followed by the rapid reforming of the formed formaldehyde to produce 2 moles of H_2 and 1 mole of CO_2. The authors [13] confirmed the presence of formaldehyde through gas analysis from the dry reaction (without added water) of n-butanol over a Pt/Al_2O_3 catalyst. Although formaldehyde was not detected in the gas analysis of this study, possibly due to its instability under hydrothermal conditions, this reaction pathway remains feasible under the conditions of this work.

Additionally, in a study on the steam reforming of n-butanol over a $Ni\text{-}CeO_2\text{-}ZrO_2\text{-}SiO_2$ composite catalyst, Varkolu et al. [33] suggested a possible dehydroformylation of the formed butanal to yield propene, carbon monoxide, and hydrogen. Subsequently, propene could undergo hydrogenation to produce propane, while carbon monoxide might undergo the water-gas shift reaction to yield carbon dioxide and hydrogen. This pathway would also result in a 1:1:2 molar ratio of propane, carbon dioxide, and hydrogen. Fig. 4b. clearly illustrates the minor formation of propene and its gradual decrease over reaction time, potentially indicating the occurrence of this pathway in our study.

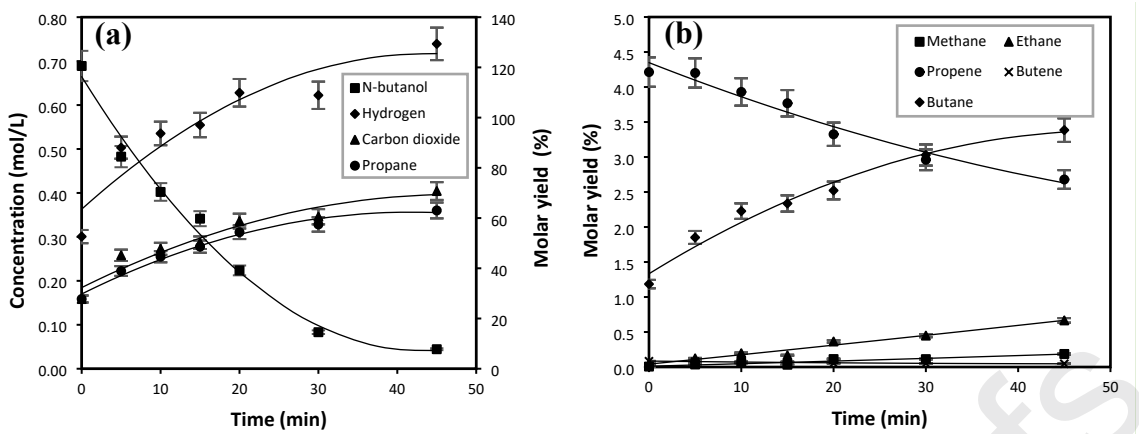

328

329 **Fig. 4.** (a) Variation of the n-butanol concentration and the molar yields of the main products;
330 (b) Variation of the molar yields of the side products. (Reaction conditions: t = 0 - 45 min, T =
331 573 K, initial N_2 pressure = 5 bar, Pt/Al_2O_3 loading = 0.5 g)

332 It is important to note that minor variations are observed in the molar yield ratios of the main
333 products compared to those anticipated from the reaction stoichiometry predicted by Equation
334 (8). These variations can be attributed to the minor occurrence of side reactions during the
335 hydrothermal processing of n-butanol over Pt/Al_2O_3 (Table 1). One plausible reaction is the
336 reforming of n-butanol to produce carbon dioxide and hydrogen in 1:3 molar ratio. N-butanol
337 reforming reaction over Pt/Al_2O_3 has been reported by Yadav et al. [23] at relatively higher
338 temperatures (623 - 773 K). The possible catalytic reforming of n-butanol could potentially
339 explain the slightly higher average molar ratio of carbon dioxide to propane (~1.07) observed
340 in this present study.

341 Furthermore, Fig. 4b, which depicts the formation of side products, indicates that a series of
342 possible hydrogen-consuming reactions occurred during the hydrothermal processing of n-
343 butanol over Pt/Al_2O_3. These potential side reactions are listed in Table 1. One such reaction
344 is the formation of butane, which increased with reaction time. A possible mechanism leading
345 to butane formation is dehydration of the n-butanol to butene over the acid sites of alumina
346 followed by hydrogenation of butene to butane over Pt metallic sites [20]. In this study, this
347 pathway was supported by the gradual decrease in butene and increase in butane molar yields
348 over time (Fig. 4b). Direct C–O hydrogenolysis of n-butanol to butane has also been proposed
349 in literature [34]. The formation of propene may result from the hydrogenolysis of terminal C-
350 C bonds in butene [16] and/or the dehydroformylation of butanal, as described earlier.
351 Isomerisation of terminal butenes to internal butenes followed by cross-metathesis with ethene
352 to produce propene has also been reported over catalytic systems comprising H-ZSM-5, H
353 Ferrierite, and tungsten on acid-washed SiO_2/Al_2O_3 [35]. Propene hydrogenation to propane is
354 also plausible, as evidenced by its gradual decrease over reaction time (Fig. 4b). The formation
355 of propene and its subsequent hydrogenation to propane supports the findings of Diejomaoh et
356 al. [16], who proposed additional propane-forming reactions alongside the main mechanism(s)
357 described earlier for the hydrothermal processing of n-butanol over Pt/Al_2O_3. The trace
358 formation of methane and ethane, along with their gradual increase over time, can be attributed
359 to the potential hydrogenolytic cracking of C_3 and C_4 gases, notably propane due to its
360 abundance in the products. Methane could also be formed by methanation reactions of CO_2 and
361 CO [16]. These minor hydrogen-consuming reactions could potentially account for the lower
362 observed molar ratios of hydrogen to carbon dioxide (1.89) and propane (2.03), compared to
363 what is expected from the combination of Equation (8) and n-butanol reforming in our study.

Table 1. Plausible main and side reactions during hydrothermal reaction of n-butanol in this study.

Main reaction(s)	Ref	Side reactions	Ref
$C_4H_9OH \xrightarrow{\text{dehydrogenation}} C_3H_7CHO+H_2$ $C_3H_7CHO \xrightarrow{\text{decarbonylation}} C_3H_8+CO$ $CO+H_2O \xrightarrow{\text{WGS}} CO_2+H_2$	[16, 19, 20, 31, 32]	$C_4H_9OH+7H_2O \xrightarrow{\text{Reforming}} 4CO_2+12H_2$	[23]
$C_4H_9OH \xrightarrow{\text{deformylation}} C_3H_8+ HCHO$ $HCHO+H_2O \xrightarrow{\text{dehydrogenation}} CO_2+2H_2$	[16]	$C_4H_9OH \xrightarrow{\text{Dehydration}} C_4H_8+H_2O$ $C_4H_8+H_2 \xrightarrow{\text{hydrogenation}} C_4H_{10}$	[16, 20]
$C_4H_9OH \xrightarrow{\text{dehydrogenation}} C_3H_7CHO+H_2$ $C_3H_7CHO \xrightarrow{\text{dehydroformyl.}} C_3H_6+CO+H_2$ $C_3H_6+H_2 \xrightarrow{\text{Hydrogenation}} C_3H_8$ $CO+H_2O \xrightarrow{\text{WGS}} CO_2+H_2$	[33]	$C_4H_8 + H_2 \xrightarrow{\text{Hydrogenolysis}} C_3H_6 + CH_4$ $C_3H_6+H_2 \xrightarrow{\text{Hydrogenation}} C_3H_8$	[16]
		$C_nH_{2n+2}+H_2 \xrightarrow{\text{Hydrogenolytic cracking}}$ shorter chain alkanes	[16]
		$CO+4H_2 \xrightarrow{\text{Methanation}} CH_4+H_2O$ $CO_2+4H_2 \xrightarrow{\text{Methanation}} CH_4+2H_2O$	[16]

It should also be noted that the deviations observed in Fig. 4 can be attributed to the challenge of accurately controlling the selectivity of the main reaction at elevated temperatures, in which case, side reactions including C-C bond cleavage may become prominent. For instance, regarding the trend in H_2 yield, the deviations could have been more pronounced due to various side reactions that affect both its formation and consumption. In this regard, competing reactions such as n-butanol dehydration/hydrogenation to form butane can initially lower the observed H_2 yield compared to the expected values from equation (8). Over time, additional minor side reactions, such as n-butanol reforming, may contribute to an increase in H_2 yield at extended reaction times.

3.2.1. Effect of temperature on n-butanol conversion and products yield

The effect of temperature on the conversion of n-butanol and the molar yield of products is investigated using 0.5 g of 5wt% Pt/Al_2O_3 at temperatures of 523 K, 548 K, and 573 K. Similar to the previous section, reaction times ranged from 0 min to 45 min, with '0 min' denoting

experiments that were promptly quenched upon reaching the set temperature. The temperature range was chosen based on the study of Diejomaoh et al. [16] that showed the highest propane selectivity among hydrocarbons obtained within this range reaching up to 92.1% at 573 K.

Fig. 5 depicts the effect of temperature on the concentration of n-butanol and the main products (propane, hydrogen and carbon dioxide) molar yield. As expected, decreasing the temperature resulted in lower n-butanol conversion and a decrease in the products molar yield. At 573 K, the conversion of n-butanol was nearly complete, reaching 97.03% after 45 min of reaction time. In comparison, at 548 K and 523 K, the conversion rates were lower, with values of 84.79% and 58.29%, respectively.

Correspondingly, the highest molar yields of propane (63.03%), hydrogen (129.36%), and carbon dioxide (70.77%) were obtained at 45 min and 573 K. As expected, these yields decreased at 548 K, with values of 51.04% for propane, 107.05% for hydrogen, and 52.75% for carbon dioxide. Finally, the lowest molar yields were obtained at 523 K, with values of 34.51% for propane, 72.11% for hydrogen, and 38.46% for carbon dioxide. The observed trends aligns well with the findings of Diejomaoh et al. [16], who demonstrated that the highest conversion of n-butanol and yield of gaseous products occurred at 573 K when using Pt/Al_2O_3 in the hydrothermal processing of n-butanol.

Furthermore, the trends in the variation of n-butanol concentration and the molar yields of the main products closely followed the reaction pathway proposed by Equation (8) at all temperatures investigated. As discussed in section 3.2, the deviations of the experimental data from the fitted curves at 573 K are primarily due to the difficulty of maintaining reaction selectivities due to promotion of side reactions at elevated temperatures. The H_2 yield may also be more affected by the occurrence of minor side reactions that contribute to both the consumption and production of H_2.

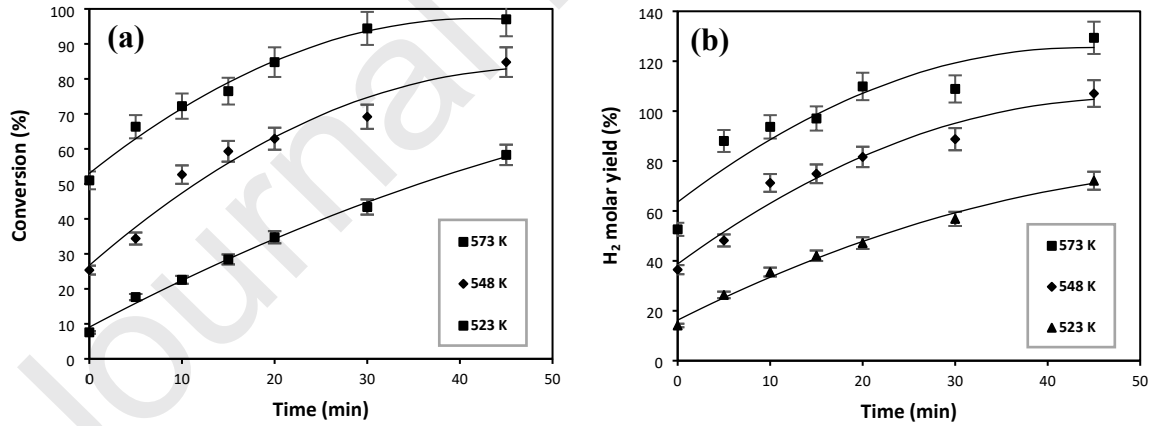

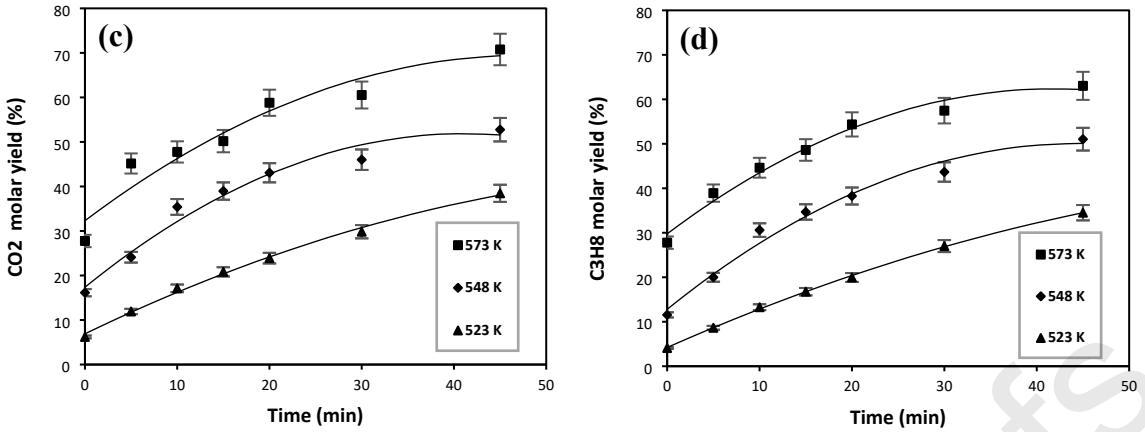

405

406 **Fig. 5.** Effect of tempreture on (a) n-butanol conversion and molar yields of (b) hydrogen (c)
407 carbon dioxide and (d) propane (Reaction conditions: t = 0 - 45 min, initial N_2 pressure = 5
408 bar, Pt/Al_2O_3 loading = 0.5 g)

409 **3.3. Kinetics of n-butanol hydrothermal reaction**

410 To obtain the kinetic data, experiments with 0.5 g of 5wt% Pt/Al_2O_3 at reaction times of 0, 5,
411 10, 15, 20, 30 and 45 min and at three different temperatures of 523 K, 548 K, and 573 K is
412 conducted. The variation in n-butanol concentration with time was used to process the kinetic
413 data. In closely related studies, researchers have shown that a power-law rate equation can
414 adequately describe the rate of n-butanol reforming reaction [23, 24]. Here, an integral method
415 was used to fit the experimental data to power-law rate equation with different reaction orders.
416 Note that since water was used in excess in the reaction, the reaction order with respect to water
417 is assumed to be zero. The results showed that a reaction order of unity provided the best fit
418 for the disappearance rate of n-butanol. According to the integral method, for a constant volume
419 system, integration of a first order reaction (Equation (9)) yields the Equation (10):

$$\frac{dC_B}{dt} = kC_B \qquad (9)$$

$$\ln(C_B) = -kt + \ln(C_{B_0}) \qquad (10)$$

420 where k is the overall pseudo reaction rate constant (s^{-1}), t is the reaction time (s), C_B and C_{B_0}
421 are the recovered and initial butanol concentrations (mol L^{-1}) respectively.

422 When the model is satisfactory to describe the rate of n-butanol disappearance, a plot of ln C_B
423 vs time should provide a straight line. Fig. 6 depicts such plots for three different temperatures
424 of 523 K, 548 K, and 573 K. The slope of these plots is equal to the pseudo reaction rate
425 constant (k (s^{-1})). The values of k (s^{-1}) and their corresponding coefficient of determination
426 (R^2) is provided in Table 2. As expected, one can see an increase in the value of k with an
427 increase in temperature.

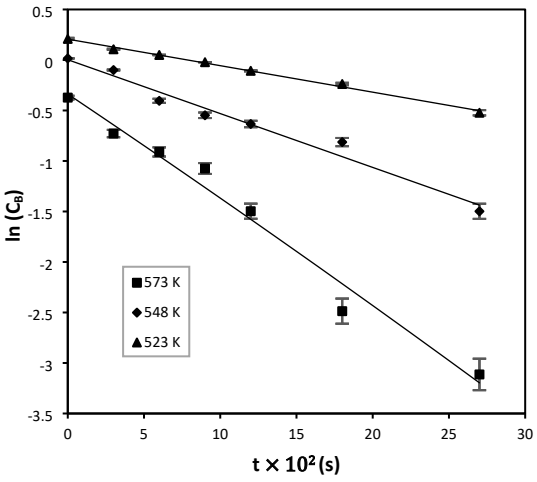

Fig. 6. Pseudo first-order reaction model of n-butanol hydrothermal reaction according to equation (10) at 523 K, 548 K, and 573 K (Reaction conditions: t = 0 - 45 min, initial N_2 pressure = 5 bar, Pt/Al_2O_3 loading = 0.5 g).

Table 2. Pseudo reaction rate constants of hydrothermal reaction of n-butanol at different temperatures.

Temperature (K)	Reaction rate constant, k × 10^{-1} (s^{-1})	R^2
573	10.59	0.9776
548	5.33	0.9732
523	2.62	0.9951

The data provided in Table 2 then is used to determine the Arrhenius activation energy by plotting the log k vs 1/T according to Equation (11):

$$\log k = \left(\frac{-E_a}{2.303R}\right)\left(\frac{1}{T}\right) + \log k_0 \qquad (11)$$

where E_a is the activation energy (J mol^{-1}), R is the gas constant (J $K^{-1}mol^{-1}$), and k_0 is pre-exponential factor (s^{-1}). From the slope and intercept of the Arrhenius plot presented in Fig. 7, the activation energy (E_a) and the pre-exponential factor (k_0) were calculated to be 69.59 kJ mol^{-1} and 2.31 × 10^3 s^{-1} respectively. The coefficient of determination for the Arrhenius plot (Fig. 7.) was R^2 = 0.9997, indicating a strong fit of the data to the Arrhenius equation.

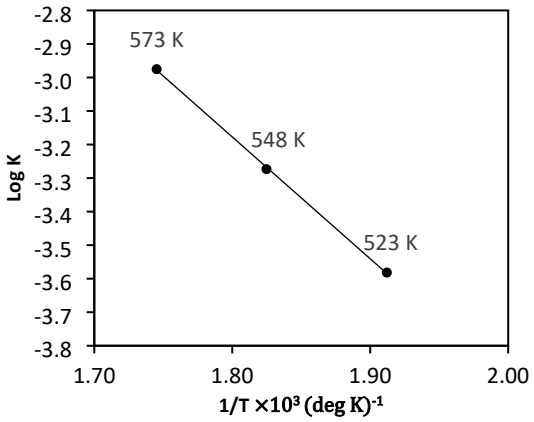

443

444 **Fig. 7.** Plot of the Arrhenius reaction rate constant vs temperature for hydrothermal reaction of
445 n-butanol.

446 To the best of our knowledge, this is the first study to evaluate the kinetics of the hydrothermal
447 reaction of n-butanol over a Pt/Al_2O_3 catalyst for the purpose of producing propane and H_2.
448 Due to the lack of literature data on the kinetics of this specific transformation, a direct
449 comparison of our results with existing data was not feasible. Nevertheless, Table 3 provides a
450 comparison of closely related kinetic studies on n-butanol steam reforming with this present
451 study.

452

453 **Table 3.** Comparison of kinetic studies on n-butanol steam reforming with this study.

Catalyst	Reaction conditions	Reaction order	E_a[a] (kJ mol^{-1})[1]	Reference
5% Ru/Al_2O_3	T = 623-773 K, S/C = 33.3 mol mol^{-1}, W/F_{A0} = 3.3-16.7 g h mol^{-1}	1.05	78	[24]
0.5% Pt/Al_2O_3	T = 623-773 K, S/C = 33.3 mol mol^{-1}, W/F_{A0} = 33.4-166.8 g h mol^{-1}	1	22.9	[23]

[1] E_a with respect to n-butanol consumption

0.5% Pd/Al_2O_3	T = 623-773 K, S/C = 33.3 mol mol^{-1}, W/F_{A0} = 33.4-166.8 g h mol^{-1}	1	30.2	[23]
Ni/Hydrotalcite	T = 623-773 K, S/C = 50.4 mol mol^{-1}, W/F_{A0} = 5-12.5 g h mol^{-1}	1	50	[25]
5% Pt/Al_2O_3	T = 523-573 K, Feed = 10wt% butanol in water, Catalyst loading = 0.5 g	1	69.59	This work

In studies on n-butanol reforming reported in the literature, there appears to be an agreement that the reaction order with respect to butanol was first-order [23-25]. Interestingly, this hydrothermal reaction study also demonstrated that a reaction order of unity best described the rate of butanol disappearance, resulting in the production of propane, H_2, and CO_2. While direct comparison of activation energies may be inadequate due to differences in reaction conditions, it is notable that the activation energy observed in this study was within a similar order of magnitude as that reported in some of the n-butanol reforming studies [24, 25].

3.3.1. Heterogeneous kinetic modelling

As previously described, the catalytic hydrothermal reaction of n-butanol in the system used for this present study is considered a gas-liquid-solid three-phase reaction, involving n-butanol and water in the gas-liquid phase, reaction intermediates (such as CO and/or HCHO) in the gas phase, and the surface of the solid catalyst. Although a simple first-order power-law rate model adequately described the rate of hydrothermal reaction of n-butanol, it was unable to provide insight into surface processes occurring on Pt/Al_2O_3 catalyst. To address this limitation, the Langmuir-Hinshelwood (LH) model emerged as a widely adopted method for deriving rate expressions in fluid-solid catalytic reactions. This mechanistic model considers both adsorption/desorption phenomena on the catalyst surface and the surface reactions.

As discussed in Section 3.2, the deformylation and dehydrogenation/decarbonylation of n-butanol were suggested as the two plausible dominant reaction mechanisms for the formation of propane, H_2, and CO_2 over a Pt/Al_2O_3 catalyst [16]. To develop a suitable LH model expression, each of these reaction mechanisms could be described in terms of four elementary reaction steps.

For the dehydrogenation/decarbonylation mechanism, the steps include the adsorption of n-butanol on the surface, followed by its reaction to produce propane gas and surface-adsorbed CO. The adsorbed CO then rapidly reacts with surface-adsorbed water to produce hydrogen and carbon dioxide. These elementary steps are depicted in Equations (12) to (15).

$$\text{Step1: } C_4H_9OH + S \underset{k_{-1}}{\overset{k_1}{\rightleftharpoons}} C_4H_9OH(S) \quad (12)$$

$$\text{Step2: } C_4H_9OH(S) \underset{k_{-2}}{\overset{k_2}{\rightleftharpoons}} CO(S) + C_3H_8 + H_2 \quad (13)$$

$$\text{Step3: } H_2O + S \underset{k_{-3}}{\overset{k_3}{\rightleftharpoons}} H_2O(S) \quad (14)$$

$$\text{Step4: } CO(S) + H_2O(S) \underset{k_{-4}}{\overset{k_4}{\rightleftharpoons}} CO_2 + H_2 + 2S \quad (15)$$

For the deformylation mechanism, the initial adsorption of n-butanol on the surface is followed by its reaction to produce propane gas and surface-adsorbed formaldehyde. The adsorbed formaldehyde then rapidly reacts with surface-adsorbed water to produce hydrogen and carbon dioxide. These elementary steps are depicted in Equations (16) to (19).

$$\text{Step1: } C_4H_9OH + S \underset{k_{-1}}{\overset{k_1}{\rightleftharpoons}} C_4H_9OH(S) \quad (16)$$

$$\text{Step2: } C_4H_9OH(S) \underset{k_{-2}}{\overset{k_2}{\rightleftharpoons}} HCHO(S) + C_3H_8 \quad (17)$$

$$\text{Step3: } H_2O + S \underset{k_{-3}}{\overset{k_3}{\rightleftharpoons}} H_2O(S) \quad (18)$$

$$\text{Step4: } HCHO(S) + H_2O(S) \underset{k_{-4}}{\overset{k_4}{\rightleftharpoons}} CO_2 + 2H_2 + 2S \quad (19)$$

Rate expressions were derived by assuming either the adsorption or surface reaction of n-butanol as the rate-determining step (RDS). The rapid reaction of water with CO or

formaldehyde excludes these as RDS [16]. Simplifying assumptions, given the negligible concentration of products relative to water, resulted in identical rate expressions for both mechanisms: one based on n-butanol adsorption (Model 1) and the other on its surface reaction (Model 2) (see *Supplementary Information Section S1*). These rate expressions are depicted in Equations (20) and (21), respectively.

$$\text{Model 1: } r = \frac{k_1 C_B}{1 + K_3 C_W} \tag{20}$$

$$\text{Model 2: } r = \frac{K_1 k_2 C_B}{1 + K_1 C_B + K_3 C_W} \tag{21}$$

k_n is defined as the forward reaction rate constant (mol g^{-1} s^{-1})[2], the equilibrium constant K_n is defined as the ratio of the forward reaction rate constant to the backward reaction rate constant. C_B and C_W represent the concentrations of n-butanol and water (mol L^{-1}), respectively.

The model variables including the surface reaction rate constant (k_s), n-butanol equilibrium constant (K_1), and water equilibrium constant (K_3) were estimated using a nonlinear generalized reduced gradient (GRG) solver in Microsoft Excel. The model was solved by minimizing the objective function, which is the residual sum of squares (RSS) as defined in Equation (22):

$$RSS = \sum (r_{exp} - r_{mod})^2 \tag{22}$$

where r_{exp} and r_{mod}denote the experimental and the model-computed reaction rates, respectively. To identify the best-fit model and hence determine the rate-determining step that describes the kinetics of the n-butanol hydrothermal reaction, the R^2 value is calculated using Equation (23):

$$R^2 = 1 - \frac{\sum (r_{exp} - r_{mod})^2}{\sum (r_{exp} - r_{exp,avg})^2} \tag{23}$$

Table 4 summarizes the estimated values of reaction rate constants and their corresponding R^2 value at different reaction temperatures. As can be seen, Model 2 with R^2 values between

[2] Here, the rates are expressed in units of mol g^{-1} s^{-1}, considering a catalyst loading of 0.04 g L^{-1}in all experiments.

0.9412 and 0.999 clearly provided more accurate fit to the experimental data than Model 1 with R^2 values of between 0.8727 and 0.9751. Additionally, as shown in Table 5, the activation energy estimated by Model 2 closely approximated that obtained from the power law model (69.59 kJ mol^{-1}). Hence, Model 2 was considered a better fit and is subjected to further evaluation.

Table 4: Estimation of Model 1 and Model 2 parameters at different temperatures.

Model	Temperature (K)	$k \times 10^{-4}$ (mol $g^{-1}s^{-1}$)	K_1	K_3	R^2
1	573	17.37	-	0.54	0.8727
	548	12.05	-	0.56	0.9527
	523	6.68	-	0.62	0.9751
2	573	2.46	6.85	0.45	0.9412
	548	1.49	8.56	0.47	0.9479
	523	0.71	10.70	0.50	0.9990

Table 5: Estimation of Arrhenius activation energy and pre-exponential factor for Model 1 and 2.

Model	k_0 (mol $g^{-1}s^{-1}$)	E_{act} (kJ mol^{-1})	R^2
1	1.67	36.95	0.9931
2	44.09	62.46	0.9936

As per Boudart et al. [36], the equilibrium constants reported in a proposed L-H model must follow the thermodynamic criteria outlined in Equation (24) to hold a physical meaning and thus validate the proposed reaction model.

$$10 \leq -\Delta S \leq 12.2\text{-}0.0014\Delta H \qquad (24)$$

where ΔS is the entropy of adsorption for the substrate (cal mol^{-1} K^{-1}) and ΔH is the enthalpy of adsorption for the substrate (cal mol^{-1}).

The entropy (ΔS) and enthalpy (ΔH) values for the adsorption of butanol and water were calculated utilizing Van't Hoff's equation provided in Equation (25):

$$\ln K = -\frac{\Delta H}{RT} + \frac{\Delta S}{R} \qquad (25)$$

where K is the adsorption equilibrium constant for either butanol or water, R is the gas constant and T is the absolute temperature.

The estimated values for Model 2 are shown in Table 6. It can be seen that Model 2 follows the guidelines for both reactants as suggested by Boudart et al. [36] in Equation (24). The obtained values indicated that Model 2 was thermodynamically consistent and supported the proposed L-H reaction model in this study. Examining the magnitude of the estimated enthalpy of adsorption for n-butanol and water in Table 6 suggests that both reactants adsorbed weakly onto the catalyst surface, as substantially higher values would suggest stronger interactions.

Table 6: Estimation of the thermodynamic parameters for model 2.

Substrate	ΔH (kJ mol^{-1})	ΔS (kJ mol^{-1} K^{-1})	R^2	Rule 1 proposed in Equation (24)[3].	Rule 2 proposed in Equation (24)
Butanol	-33.51	-0.044	0.9993	$10 \leq 10.58$ (Yes)	$10.58 \leq 23.41$ (Yes)
Water	-18.16	-0.045	0.9993	$10 \leq 10.77$ (Yes)	$10.77 \leq 18.28$ (Yes)

Similar low values of enthalpy of adsorption for n-butanol and water have been reported over Ru/Al_2O_3 catalysts [24]. The parity plot for Model 2 is shown in Fig. 8. Same as the power rate law, the accuracy of the L-H model was higher at lower temperatures investigated and tended to decrease as temperature increased. This was possibly due to the occurrence of minor side reactions discussed in Section 3.2 and/or the limitation of collecting highly accurate data in a

[3] Note that the adsorption values in equation (24) are in calories.

batch system. Nevertheless, the average R^2 value of Model 2 across different temperature were 0.9625 that shows a reasonable agreement of the predicted and experimental reaction rates.

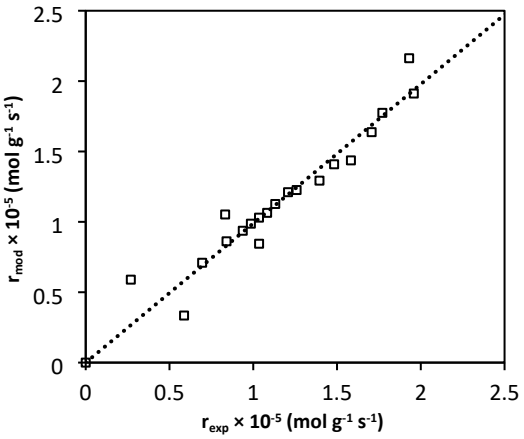

Fig. 8. Parity Plot of model 2 for comparison of predicted and experimental reaction rates.

The activation energy estimated by Model 2 and the power rate law are notably higher than the typical activation energy observed in a mass transfer-limited system ($12-21$ kJ mol^{-1}), suggesting that the experimental data were collected within the kinetically controlled regime [37-40]. The obtained values for the activation energy further supported the conclusion of minimal internal and external mass transfer limitation, as discussed in Section 3.1. The proposed L-H model was applicable to both dominant reaction mechanism proposed in the literature [16] for the formation of propane, H_2, and CO_2 over Pt/Al_2O_3 catalyst and under the reaction condition used in our study.

4. Conclusions

This study systematically examined the hydrothermal reaction of n-butanol with 1.5 mol L^{-1} n-butanol initial concentration over 5wt% Pt/Al_2O_3 at various reaction temperatures (523 K - 573 K) and reaction times (0 - 45 minutes) using a batch reactor to collect kinetic data. Experiments were conducted with different catalyst loadings (0.1 g to 1 g), and it was found that external mass transfer was negligible. Additionally, analysis of the Weisz-Prater criteria indicated the absence of internal mass transfer for the conditions of the study. Gas product analysis over 45 minutes of reaction time showed that the formation of the main products could be reliably described by the reaction pathway represented by Equation (8).

The experimental data was fitted to a power-law rate equation using an integral method, revealing a reaction order of unity with respect to n-butanol and an activation energy of 69.59 kJ mol^{-1}. Langmuir-Hinshelwood models were established based on two plausible dominant reaction mechanisms of dehydrogenation/decarbonylation and deformylation, assuming either the adsorption or surface reaction of n-butanol as the rate-determining step. Simplifying assumptions, due to the negligible concentration of products relative to water, resulted in identical rate expressions for both mechanisms. A statistical approach revealed that Model 2 (n-butanol surface reaction as RDS) provided a better fit to the experimental data with R^2 values between 0.9412 and 0.999. The activation energy predicted by Model 2 was 62.46 kJ mol^{-1} which was close to that of power law. The proposed L-H method was found to be thermodynamically consistent and examining the magnitude of the estimated enthalpy of

adsorption for n-butanol and water suggested that both reactants adsorbed weakly onto the catalyst surface.

It should be noted that while this study proved the prevailing overall reaction equation involved in the conversion of n-butanol, it was unable to distinguish between the two mechanisms of butanol dehydrogenation/decarbonylation and deformylation. This was possibly due to the fast rate of conversion of the side products, namely CO and HCHO within the hydrothermal reaction system used in this present study. Making a distinction between the two mechanisms could be better served using a continuous rig equipped with a real-time sampling facility. The kinetic results presented in this paper can be a reference for predicting the reaction behaviour of n-butanol hydrothermal reaction over Pt/Al_2O_3catalyst and the design of a catalytic reactor.

Funding: The authors would like to thank Futuria Fuels, SHV Energy, The Netherlands for PhD studentship for S.E.H.

Credit authorship contribution statement.

Seyed Emad Hashemnezhad: Investigation, Methodology, Data Curation, Validation, Visualization, Writing original draft. **Jude A. Onwudili:** Conceptualization, Funding acquisition, Methodology, Visualization, Supervision, Project administration, Writing original draft, Writing - review & editing. **Patricia Thornley:** Supervision, Resources, Project administration, Visualisation, Writing – review & editing. **Keith E. Simons:** Supervision, Resources, Project administration, Validation, Writing – review & editing.

Declaration of competing interest:

The authors declare the following financial interests/personal relationships which may be considered as potential competing interests: **Jude Onwudili** reports that financial support was provided by SHV Energy, The Netherlands. **Keith Simons**, a co-author of this paper, works for Futuria Fuels, SHV Energy, The Netherlands and was involved in design of study and the decision to publish the results.

Data availability:

Data will be made available on request.

Appendix A. Supplementary material

References

[1] P.M. Forster, C. Smith, T. Walsh, W.F. Lamb, R. Lamboll, B. Hall, M. Hauser, A. Ribes, D. Rosen, N.P. Gillett, M.D. Palmer, J. Rogelj, K. von Schuckmann, B. Trewin, M. Allen, R. Andrew, R.A. Betts, A. Borger, T. Boyer, J.A. Broersma, C. Buontempo, S. Burgess, C. Cagnazzo, L. Cheng, P. Friedlingstein, A. Gettelman, J. Gütschow, M. Ishii, S. Jenkins, X. Lan, C. Morice, J. Mühle, C. Kadow, J. Kennedy, R.E. Killick, P.B. Krummel, J.C. Minx, G. Myhre, V. Naik, G.P. Peters, A. Pirani, J. Pongratz, C.F. Schleussner, S.I. Seneviratne, S. Szopa, P. Thorne, M.V.M. Kovilakam, E. Majamäki, J.P. Jalkanen, M. van Marle, R.M. Hoesly, R. Rohde, D. Schumacher, G. van der Werf, R. Vose, K. Zickfeld, X. Zhang, V. Masson-Delmotte, P. Zhai, Indicators of Global Climate Change 2023: annual update of key indicators of the state of the climate system and human influence, Earth Syst. Sci. Data 16(6) (2024) 2625-2658. https://doi.org/10.5194/essd-16-2625-2024.

[2] WLGA, The role of LPG in shaping the energy transition, 2018. https://www.worldliquidgas.org/wp-content/uploads/2018/10/The-role-of-LPG-in-shaping-the-energy-transition-2018.pdf. (Accessed 17 July 2024).

[3] Autogas.net, Will our clean air stay? Autogas can help! https://auto-gas.net/why-autogas/airquality/. (Accessed 17 July 2024).

[4] WLGA, Heating. https://www.worldliquidgas.org/key-focus-areas/heating/. (Accessed 1 July 2024).

[5] WLGA, What is Liquid Gas? https://www.worldliquidgas.org/about-liquid-gas/what-is-liquid-gas/. (Accessed 12 June 2024).

[6] WLGA, EXCEPTIONAL ENERGY. https://www.worldliquidgas.org/key-focus-areas/exceptional-energy/. (Accessed 12 June 2024).

[7] Atlantic Consulting, BioLPG: A survey of markets, feedstocks, process technologies, projects and environmental impacts., 2018, p. 52.

[8] WLGA, The Role of LPG and bioLPG in Europe, 2019. https://www.worldliquidgas.org/wp-content/uploads/2020/03/The-Role-of-LPG-Bio-LPG-in-Europe-The-2019-Report.pdf. (Accessed 12 June 2024).

[9] Liquid Gas UK, A Practical Approach-Analysis of Off-Grid Heat Decarbonisation Pathways, 2019.

[10] E.M. Lucy Hopwood, Sotirios Sourmelis, Biopropane: Feedstocks, Feasibility and our Future Pathway, NNFCC, 2019, September.

[11] I. Razaq, K.E. Simons, J.A. Onwudili, Parametric Study of Pt/C-Catalysed Hydrothermal Decarboxylation of Butyric Acid as a Potential Route for Biopropane Production, Energies 14(11) (2021). https://doi.org/10.3390/en14113316.

[12] J. Jiang, T. Li, K. Huang, G. Sun, J. Zheng, J. Chen, W. Yang, Efficient Preparation of Bio-based n-Butane Directly from Levulinic Acid over Pt/C, Industrial & Engineering Chemistry Research 59(13) (2020) 5736-5744. https://doi.org/10.1021/acs.iecr.0c00255.

[13] K. Murata, I. Takahara, M. Inaba, Propane formation by aqueous-phase reforming of glycerol over Pt/H-ZSM5 catalysts, Reaction Kinetics and Catalysis Letters 93(1) (2008) 59-66. https://doi.org/10.1007/s11144-008-5190-0.

[14] C.T. Alves, J.A. Onwudili, Screening of Nickel and Platinum Catalysts for Glycerol Conversion to Gas Products in Hydrothermal Media, Energies 15(20) (2022). https://doi.org/10.3390/en15207571.

[15] K.E. Simons, H.V. Rensburg, EP4259325A2, 2022.

[16] O.T. Abafe Diejomaoh, J.A. Onwudili, K.E. Simons, P. Maziero, On-purpose production of propane fuel gas from the hydrothermal reactions of n-butanol over Pt/Al2O3 catalyst: A parametric and mechanistic study, Fuel 365 (2024) 131140. https://doi.org/https://doi.org/10.1016/j.fuel.2024.131140.

[17] H.G. Moon, Y.-S. Jang, C. Cho, J. Lee, R. Binkley, S.Y. Lee, One hundred years of clostridial butanol fermentation, FEMS Microbiology Letters 363(3) (2016). https://doi.org/10.1093/femsle/fnw001.

[18] H. Choi, J. Han, J. Lee, Renewable Butanol Production via Catalytic Routes, International journal of environmental research and public health 18(22) (2021). https://doi.org/10.3390/ijerph182211749.

[19] A. Wawrzetz, B. Peng, A. Hrabar, A. Jentys, A.A. Lemonidou, J.A. Lercher, Towards understanding the bifunctional hydrodeoxygenation and aqueous phase reforming of glycerol, Journal of Catalysis 269(2) (2010) 411-420. https://doi.org/10.1016/j.jcat.2009.11.027.

[20] B. Peng, C. Zhao, I. Mejía-Centeno, G.A. Fuentes, A. Jentys, J.A. Lercher, Comparison of kinetics and reaction pathways for hydrodeoxygenation of C3 alcohols on Pt/Al2O3, Catalysis Today 183(1) (2012) 3-9. https://doi.org/10.1016/j.cattod.2011.10.022.

[21] E. Girel, A. Cabiac, A. Chaumonnot, M. Besson, A. Tuel, Selective Carbon Deposition on γ-Alumina Acid Sites: toward the Design of Catalyst Supports with Improved Hydrothermal Stability in Aqueous Media, ACS Applied Materials & Interfaces 12(11) (2020) 13558-13567. https://doi.org/10.1021/acsami.0c01646.

[22] A.P. Amrute, K. Jeske, Z. Łodziana, G. Prieto, F. Schüth, Hydrothermal Stability of High-Surface-Area α-Al2O3 and Its Use as a Support for Hydrothermally Stable Fischer–Tropsch Synthesis Catalysts, Chemistry of Materials 32(10) (2020) 4369-4374. https://doi.org/10.1021/acs.chemmater.0c01587.

[23] A.K. Yadav, P.D. Vaidya, A study on the efficacy of noble metal catalysts for butanol steam reforming, International Journal of Hydrogen Energy 44(47) (2019) 25575-25588. https://doi.org/https://doi.org/10.1016/j.ijhydene.2019.07.191.

[24] A.K. Yadav, P.D. Vaidya, Kinetic investigation on butanol steam reforming over Ru/Al2O3 catalyst, International Journal of Hydrogen Energy 42(40) (2017) 25203-25212. https://doi.org/https://doi.org/10.1016/j.ijhydene.2017.08.021.

[25] A.K. Yadav, P.D. Vaidya, Reaction Kinetics of Steam Reforming of n-Butanol over a Ni/Hydrotalcite Catalyst, 41(5) (2018) 890-896. https://doi.org/https://doi.org/10.1002/ceat.201600738.

[26] J.A. Onwudili, C.A. Scaldaferri, Catalytic upgrading of intermediate pyrolysis bio-oil to hydrocarbon-rich liquid biofuel via a novel two-stage solvent-assisted process, Fuel 352 (2023) 129015. https://doi.org/https://doi.org/10.1016/j.fuel.2023.129015.

[27] J.A. Onwudili, I. Razaq, K.E. Simons, Optimisation of Propane Production from Hydrothermal Decarboxylation of Butyric Acid Using Pt/C Catalyst: Influence of Gaseous Reaction Atmospheres, Energies 15(1) (2021). https://doi.org/10.3390/en15010268.

[28] P.B. Weisz, C.D. Prater, Interpretation of Measurements in Experimental Catalysis, in: W.G. Frankenburg, V.I. Komarewsky, E.K. Rideal (Eds.), Advances in Catalysis, Academic Press1954, pp. 143-196. https://doi.org/https://doi.org/10.1016/S0360-0564(08)60390-9.

[29] C.R. Wilke, P. Chang, Correlation of diffusion coefficients in dilute solutions, 1(2) (1955) 264-270. https://doi.org/https://doi.org/10.1002/aic.690010222.

[30] A. Kirilin, J. Wärnå, A. Tokarev, D.Y. Murzin, Kinetic Modeling of Sorbitol Aqueous-Phase Reforming over Pt/Al2O3, Industrial & Engineering Chemistry Research 53(12) (2014) 4580-4588. https://doi.org/10.1021/ie403813y.

[31] B. Roy, H. Sullivan, C.A. Leclerc, Effect of variable conditions on steam reforming and aqueous phase reforming of n-butanol over Ni/CeO2 and Ni/Al2O3 catalysts, Journal of Power Sources 267 (2014) 280-287. https://doi.org/10.1016/j.jpowsour.2014.05.090.

[32] B. Roy, H. Sullivan, C.A. Leclerc, Aqueous-phase reforming of n-BuOH over Ni/Al2O3 and Ni/CeO2 catalysts, Journal of Power Sources 196(24) (2011) 10652-10657. https://doi.org/10.1016/j.jpowsour.2011.08.093.

[33] M. Varkolu, A. Kunamalla, S.A.K. Jinnala, P. Kumar, S.K. Maity, D. Shee, Role of CeO2/ZrO2 mole ratio and nickel loading for steam reforming of n-butanol using Ni–CeO2–ZrO2–SiO2 composite catalysts: A reaction mechanism, International Journal of Hydrogen Energy 46(10) (2021) 7320-7335. https://doi.org/https://doi.org/10.1016/j.ijhydene.2020.11.240.

[34] E.I. Gürbüz, D.D. Hibbitts, E. Iglesia, Kinetic and Mechanistic Assessment of Alkanol/Alkanal Decarbonylation and Deoxygenation Pathways on Metal Catalysts, Journal of the American Chemical Society 137(37) (2015) 11984-11995. https://doi.org/10.1021/jacs.5b05361.

[35] Y. Shi, A.S. Weller, A.J. Blacker, P.W. Dyer, Conversion of butanol to propene in flow: A triple dehydration, isomerisation and metathesis cascade, Catalysis Communications 164 (2022). https://doi.org/10.1016/j.catcom.2022.106421.

[36] M. Boudart, D. Mears, M.J.I.C.B. Vannice, In congres international chimie industrielle, 32 (1967) 281.

[37] E. Aliu, A. Hart, J. Wood, Kinetics of Vanillin Hydrodeoxygenation Reaction in an Organic Solvent Using a Pd/C Catalyst, Industrial & Engineering Chemistry Research 58(33) (2019) 15162-15172. https://doi.org/10.1021/acs.iecr.9b02907.

[38] E. Crezee, B.W. Hoffer, R.J. Berger, M. Makkee, F. Kapteijn, J.A.J.A.C.A.-g. Moulijn, Three-phase hydrogenation of d-glucose over a carbon supported ruthenium catalyst—mass transfer and kinetics, 251 (2003) 1-17.

[39] C. de Bellefon, N. Tanchoux, S. Caravieilhes, New reactors and methods for the investigation of homogeneous catalysis, Journal of Organometallic Chemistry 567(1) (1998) 143-150. https://doi.org/https://doi.org/10.1016/S0022-328X(98)00677-9.

[40] N. Déchamp, A. Gamez, A. Perrard, P. Gallezot, Kinetics of glucose hydrogenation in a trickle-bed reactor, Catalysis Today 24(1) (1995) 29-34. https://doi.org/https://doi.org/10.1016/0920-5861(95)00019-C.

- Kinetics of n-butanol hydrothermal reactions over 5wt% Pt/Al_2O_3 were investigated.
- Propane, CO_2 and hydrogen obtained as main products in 1:1:2 molar ratios.
- Deformylation and/or decarbonlyation of n-butanol as dominant reaction mechanisms.
- N-butanol first-order reaction with activation energy of 70 kJ mol^{-1} by Power-law.
- Langmuir-Hinshelwood model predicted similar activation energy of 62 kJ mol^{-1}.
- Potential to develop a large-scale high-yielding biopropane production process.

Declaration of interests

☐ The authors declare that they have no known competing financial interests or personal relationships that could have appeared to influence the work reported in this paper.

☒ The authors declare the following financial interests/personal relationships which may be considered as potential competing interests: **Jude Onwudili** reports that financial support was provided by SHV Energy, The Netherlands. **Keith Simons**, a co-author of this paper, works for Futuria Fuels, SHV Energy, The Netherlands and was involved in design of study and the decision to publish the results.